The nature of the chemical bonding in the D_{3h} and C_{2v} isomers of $Fe_3(CO)_{12}$

Hilaire Chevreau, Cyril Martinsky, Alain Sevin, Christian Minot and Bernard Silvi

Laboratoire de Chimie Théorique (CNRS UMR 7616), Université Pierre et Marie Curie, 4 Place Jussieu, 75252, Paris cedex 05, France. E-mail: silvi@lct.jussieu.fr

Received (in Montpellier, France) 6th December 2002, Accepted 5th March 2003
First published as an Advance Article on the web 16th June 2003

The bonding in the D_{3h} and C_{2v} isomers of $Fe_3(CO)_{12}$ has been studied with two complementary topological approaches, namely the atoms-in-molecules (AIM) theory and the analysis of the electron localization function (ELF). Both methods indicate that the stabilization of the C_{2v} isomer is mostly due to the presence of two ligands in bridging positions, which take advantage of a rather large electron transfer from the iron atoms. Within the ELF framework, each of these latter ligands is involved in three-center (3c–4e) bonds with the two adjacent iron atoms.

1 Introduction

The $Fe_3(CO)_{12}$ structure has long been a subject of interest. The solid structure of $Fe_3(CO)_{12}$ was first elucidated in 1969 by Wei and Dahl[1] and next confirmed by Cotton and Troup.[2] The solid structure reveals two main forms from which two clusters can be extracted: on the one hand, the least stable structure has D_{3h} symmetry; on the other hand, the most stable one has C_{2v} symmetry with two Fe atoms bridged by two carbonyl groups. Recent studies were performed on the solid using X-ray diffraction[1,3,4] and C-NMR spectroscopy[5] to investigate the structural parameters of $Fe_3(CO)_{12}$. The difference in energy between both structures has been estimated to 10 kcal mol^{-1}.[4] Several theoretical studies dealing with the bonding pattern in $Fe_3(CO)_{12}$ species have also been published.[6–10] $M_2(CO)_9$ and $M_3(CO)_{12}$ (M = Fe, Ru, Os) have been recently investigated by Hunstock *et al.*[10] at the SCF MP2 and DFT levels with relativistic core pseudo-potentials. These authors show that the DFT approach provides the best agreement with experimental structures whereas MP2 fails, and that the stable $M_3(CO)_{12}$ isomer has a C_{2v} structure in the iron complex and a D_{3h} one for Ru and Os. They pointed out that "in the bridged $M_3(CO)_{12}$ clusters, the first two HOMOs are responsible for a M–(CO)–M bridge bonding which has, at the same time, a clearcut M–M antibonding nature. If the metals orbitals are diffuse (second and third rows), the M–M repulsion overwhelms the overall M–(μ–CO)–M attraction and the non-bridged structure is preferred." The antibonding character of the bridged Fe–Fe interaction has been previously pointed out on the basis of a negative overlap population between these two atoms.[8] The question of the nature of the bridged Fe atoms thus remains. The aim of our study is to investigate on the bonding in $Fe_3(CO)_{12}$ through a topological description, using the electron localization function (ELF).

2 Theoretical methods

2.1 Method of analysis

The electrons of an atom or of a molecule can be considered as belonging to an inhomogeneous continuum (electron gas) in the same manner as molecules of dioxygen or dinitrogen belong to atmospheric air. This inhomogeneous electron gas is characterized in each point of the position space of coordinates $\boldsymbol{r}$ by its density $\rho(\boldsymbol{r})$, whose knowledge determines the energy of the system according to the Hohenberg–Kohn theorem[11] as well as its linear response properties thanks to the Hellmann–Feynman theorem. In order to get some insights into chemical reactivity one has to consider other local functions such as the local softness, the local hardness and the local Fukui function[12–22] which constitute the conceptual essence of DFT. Paradoxically, none of these functions provides information on the pairing of electrons, which is the cornerstone of bonding theory. In order to recover this latter information one has to consider another local function, namely the pair composition,[23] $c_\pi(\boldsymbol{r})$, which represents the scaled ratio of the parallel and anti-parallel pair populations contained in a sampling volume around the reference point. The sampling volume is such that its electron population has a constant arbitrary value q.

$$c_\pi(r) = q^{-2/3}\frac{N_{Vq}^{\alpha\alpha}(r) + N_{Vq}^{\beta\beta}(r)}{2N_{Vq}^{\alpha\beta}(r)}$$

In this equation $N_{Vq}^{\sigma\sigma'}$ denotes the $\sigma\sigma'$ pair population calculated over the sampling volume V_q:

$$N_{Vq}^{\alpha\alpha'} = \int_{Vq}\int_{Vq} \pi^{\sigma\sigma}(r_1, r_2)\mathrm{d}r_1\mathrm{d}r_2$$

where $\pi^{\sigma\sigma}(r_1, r_2)$ denotes the probability of finding one electron with spin σ at position r_1 and another with spin σ' at r_2. The sampling volume V_q satisfies:

$$\int_{Vq}\rho(r)\mathrm{d}r = q$$

For a single anti-parallel pair $c_\pi(r) = 0$ whereas for a collection of parallel spin electrons $c_\pi(r)$ tends to infinity. It is worth noting that neither $\rho(r)$, which can be experimentally measured, nor $c_\pi(r)$ are quantities that explicitly require the knowledge of the wavefunction. It can be demonstrated[23] that the electron localization function (ELF) of Becke and Edgecombe[24] is the Lorentzian expression of an approximated

expression of $c_\pi(r)$:

$$\mathrm{ELF}(r) \approx \frac{1}{1 + c_\pi^2(r)}$$

ELF is close to one in pair regions (core shells, bonds and lone pairs) and close to zero at the border between such regions. ELF can be determined from the experimental density either by inverting the Kohn–Sham equations[25] or with the help of a functional due to Tsirelson and Stash.[26]

The electron density distribution and the electron localization function are two complementary sources of information on the bonding. The topological analysis of their gradient fields provides a convenient way to partition the molecular position space into adjacent regions bearing a strong chemical meaning. On one hand, the theory of atoms-in-molecules (AIM) due to Bader[27] considers the electron density distribution in order to define atomic basins and bond paths. On the other hand, the ELF technique[28–30] enables one to define basins associated with cores, bonds and lone pairs. The electron localization function gradient field partition yields core basins around nuclei and valence basins in the outermost regions. A valence basin is characterized by its synaptic order, which is the number of core basins with which it has a common boundary.[31,32] Accordingly, there are monosynaptic basins corresponding to lone pairs, disynaptic ones corresponding to two-centre bonds, trisynaptic basins associated with three-center bonds and so on.

Quantitatively, the topological partition enables one to perform a population analysis in terms of basin populations:

$$N(\Omega_A) = \int_{\Omega_A} \rho(r)\mathrm{d}r$$

and to analyze the variance of the basin populations

$$\sigma^2(\Omega_A) = \int_{\Omega_A} \mathrm{d}r_1 \int_{\Omega_A} \pi(r_1, r_2)\mathrm{d}r_2 - [N(\Omega_A)]^2 + N(\Omega_A)$$

where $\pi(r_1, r_2)$ is the spinless pair function.[33] It has been shown that the variance can be readily written as a sum of contributions arising from the other basins (covariance):[34]

$$\sigma^2(\Omega_A) = \sum_{B \neq A} N(\Omega_A)N(\Omega_B) - \int_{\Omega_A} \mathrm{d}r_1 \int_{\Omega_A} \pi(r_1, r_2)\mathrm{d}r_2$$

In this expression $N(\Omega_A)N(\Omega_B)$ is the number of electron pairs classically expected from the basin population whereas $N(\Omega_A, \Omega_B)$ is the actual number of pairs obtained by integration of the pair function over the basins Ω_A and Ω_B. The variance is a measure of the quantum mechanical uncertainty of the basin population, which can be interpreted as a consequence of the electron delocalization whereas the pair covariance indicates how much the population fluctuations of two given basins are correlated. Into the AIM framework Fradera *et al.*[35] have introduced atomic localization and delocalization indexes noted $\lambda(A)$ and $\delta(A,B)$, which are: defined by:

$$\lambda(A) = N(\Omega_A) - \sigma^2(\Omega_A)$$

$$\delta(A, B) = 2N(\Omega_A)N(\Omega_A) - 2 \int_{\Omega_A} \mathrm{d}r_1 \int_{\Omega_A} \pi(r_1, r_2)\mathrm{d}r_2$$

The AIM delocalization indexes are sometimes referred to as bond orders.[36,37] The notation introduced by Fradera *et al.* can be generalized to any partition in the direct space and therefore is adopted here. Within the ELF approach the core population variance and the core valence delocalization indexes can be used to decide if a given core contributes to the synaptic order of an adjacent valence basin. For example, in the LiF molecule the variances of the C(Li) and C(F) basins are 0.09 and 0.38, respectively, whereas $\delta[C(\mathrm{Li}), V(\mathrm{F})]) = 0.16$ and $\delta[C(\mathrm{F}), V(\mathrm{F})] = 0.74$.

2.2 Computational method

The *ab initio* calculations have been performed at the hybrid Hartree–Fock density functional level B3LYP[38–41] with Gaussian98 software.[42] The geometries have been optimized with the 6-311G(d)[43–46] basis set. The analysis of the ELF function has been carried out with the ToPMoD program developed in our group at the Laboratoire de Chimie Théorique de l'Université Pierre et Marie Curie[47,48] and the visualization of the ELF isosurfaces has been done with SciAn software.[49]

3 Results and discussion

3.1 Optimized geometries

The C_{2v} isomer of $Fe_3(CO)_{12}$ is calculated to be more stable than the D_{3h} one by 9.4 kcal mol^{-1}, in fair agreement with experimental data. Fig. 1 displays the D_{3h} and C_{2v} structures whereas the most important bond lengths and bond angles are reported in Table 1.

In both structures the FeC internuclear distances are larger for the apical positions than for the equatorial ones whereas the increase of the CO bond length with respect to free carbon monoxide is slightly larger in the apical case, which is counter-intuitive since one expects that a shorter metal-ligand distance would induce a larger perturbation of the ligand. In the $Fe(CO)_5$ complex, the apical FeC distance (1.8112 Å) is also larger than the equatorial one (1.8032 Å) but the CO bond length is shortened by 0.01 Åfor apical ligands and lengthened by 0.005 Å in the equatorial position.[50] However, the shrinking measured in the apical position is hardly consistent with the observed redshift of the stretching frequency.[51] The CO molecules in the bridging positions of the C_{2v} isomer appear to be significantly perturbed as their bond lengths are increased by about about 0.036 Å. The Fe–Fe internuclear distances are shorter in the C_{2v} isomer than in the D_{3h} one: 2.693 Å [Fe(1)–Fe(2) and Fe(1)–Fe(3)] and 2.577 Å [Fe(2)–Fe(3)] *versus* 2.714 Å.

In the D_{3h} isomer the apical CO are almost parallel to the C_3 axis since $\angle$CFeC = 178.7°, the angle of the equatorial CO directions, $\angle$CFeC = 105.8° is intermediate between the local octahedral symmetry and the trigonal bipyramidal geometry of $Fe(CO)_5$. The C_{2v} geometry results in a more efficient angular relaxation. On the one hand, the apical ligands on Fe(1) are slightly bent towards the barycenter of the iron atom triangle ($\angle$CFeC = 172.7°) and on the other hand the ligands on Fe(2/3) denoted as apical are in fact in an intermediate position since the angle made by their directions is 94°.

3.2 AIM analysis

Table 2 reports the atomic basin populations, the delocalization indexes,[35] the density and the Laplacian of the density

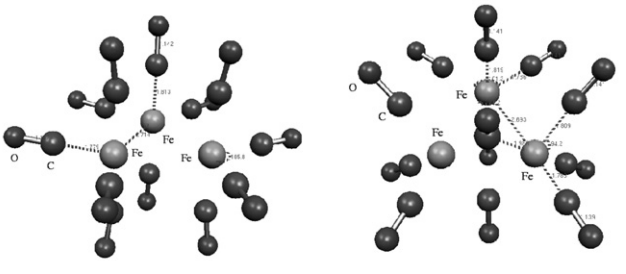

Fig. 1 Ball and stick representation of the D_{3h} (left) and C_{2v} (right) $Fe_3(CO)_{12}$ isomers.

Table 1 Optimized structural parameters of the D_{3h} and C_{2v} isomers of $Fe_3(CO)_{12}$. Bond lengths in Å, bond angles in degrees

	Apical		Equatorial			Bridging		
	FeC	CO	FeC	CO	∠CFeC	FeC	CO	∠FeCFe
D_{3h}	1.813	1.1421	1.779	1.1417	105.8			
C_{2v} Fe(1)	1.819	1.1408	1.786	1.1407	101.7			
C_{2v} Fe(2)	1.809	1.1409	1.788	1.1394		1.988	1.163	80.8

at the bond critical points for the two isomers. Within the AIM framework,[27] the structure is accounted for by the bond paths.

Fig. 2 shows the iron atomic basins and bond paths for each isomer. In the D_{3h} isomer there is a total of 3(Fe–Fe) + 12(Fe–C) + 12(C–O) bond paths, which corresponds to chemical intuition. In the C_{2v} isomer, there is no bond path between Fe(2) and Fe(3) albeit their internuclear distance is shorter than the Fe(1)–Fe(2/3) ones. This result confirms the conclusion of the orbital analysis showing an antibonding character of the Fe(2)–Fe(3) interaction.[8,10] Each bridging carbon is tricoordinated since it forms a bond path with both Fe(2) and Fe(3).

At the Fe–Fe bond critical points, $\rho(r_c)$ is very weak and $\nabla^2\rho(r_c)$ is weak and positive: such values characterize a closed shell interaction and, more precisely, metallic bonds (in small clusters).[52] The density at the Fe–C bond critical points is larger than for Fe–Fe and the Laplacian is positive and large, which are the AIM signature of dative bonds. Finally, the large values of the indicators for CO can be interpreted as the consequence of the rather large weight of the ionic contribution, which is enhanced by the back donation [$\nabla^2\rho(r_c)$ is twice the free carbon monoxide value].

The analysis of the atomic populations indicates a net electron transfer towards the ligands, which ranges from 0.10e [equatorial ligand of Fe(2) in the C_{2v} isomer] to 0.32e (bridging ligand). The transfers are larger for apical ligands than for equatorial ones and for the D_{3h} structure than for the C_{2v} one. Within the CO moiety, the carbon population is increased upon complexation by the net transfer from the metal and also by a small transfer from the oxygen. The delocalization indexes, which are sometimes interpreted in terms of bond orders,[37] are rather small for Fe–Fe interactions, of the order of 1 for FeC and of 1.6 for CO. It is worth noting that the back donation yields a decrease of δ(C,O) with respect to free CO of about 0.20.

Table 2 Atomic populations $N(A)$, delocalization indexes $\delta(A,B)$, $\rho(r_c)$ and density Laplacian $\nabla^2\rho(r_c)$ at bond critical points

	$N(A)$	$N(B)$	$\delta(A,B)$	$\rho(r_c)$	$\nabla^2\rho(r_c)$
Free CO					
C–O	4.87	9.12	1.80	0.5067	0.2163
***D*$_{3h}$**					
Fe–Fe	25.35		0.40	0.0349	0.0133
Fe–C(ap)		5.09	0.96	0.1388	0.5196
C–O (ap)		9.09	1.60	0.4718	0.5120
Fe–C(eq)		5.07	1.06	0.1589	0.5248
C–O (eq)		9.08	1.62	0.4720	0.4964
***C*$_{2v}$**					
Fe(1)Fe(2)	25.39	25.34	0.42	0.0370	0.0116
Fe(2)Fe(3)			0.26		
Fe(1)C(ap)		5.04	0.94	0.1373	0.5187
C–O (ap)		9.12	1.58	0.4734	0.5084
Fe(1)C(eq)		5.03	1.04	0.1509	0.5286
C–O (eq)		9.09	1.62	0.4730	0.5236
Fe(2)C(ap)		5.04	0.98	0.1419	0.5247
C–O (ap)		9.09	1.60	0.4731	0.5105
Fe(2)C(eq)		5.03	1.04	0.1479	0.5556
C–O (eq)		9.07	1.64	0.4744	0.5332
Fe(2)C(br)		5.24	1.28	0.1011	0.2413
C–O (br)		9.08	1.54	0.4486	0.3857

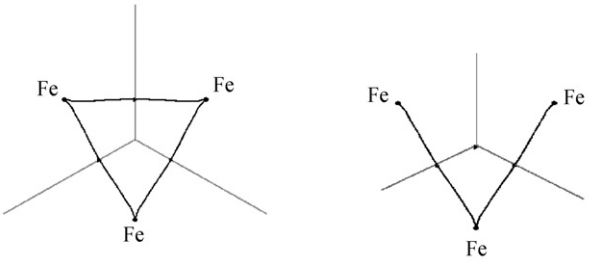

Fig. 2 Bond paths and atoms basins of the Fe_3 cluster: D_{3h} (left) and C_{2v} (right).

3.3 ELF analysis

The irreducible localization domains of the $Fe_3(CO)_{12}$ isomers are displayed in Fig. 3. In the ELF picture, the complex can be considering as twelve CO ligands linked to a Fe_3 cluster. The electron density associated to each ligand is partitioned into five basins corresponding to the carbon C(C) and oxygen C(O) cores, to the FeC dative bond V(Fe, C), to the CO bond V(C, O) and to the oxygen lone pairs V(O). The cluster part of the D_{3h} structure has 3 core basins, C(Fe), and 3 disynaptic valence basins, V(Fe, Fe), as shown in Fig. 4. In the C_{2v} isomer, there is one less valence basin: that between Fe(2) and Fe(3) is missing.

The populations of the iron core basins are very close for both isomers: 23.50 for D_{3h} and 23.47 for C_{2v}, which corresponds to a local [Ar]d^6 configuration since the missing density of 1.5e is located in the V(Fe, Fe) valence basins. The population of these latter basins, 0.65 for D_{3h} and 0.55 for C_{2v}, is not consistent with a picture in which the iron atoms form covalent bonds between themselves. The superposition of resonance structures seems more satisfactory and is supported by the large values of the variance of the V(Fe,Fe) populations compared to the populations themselves. For the D_{3h} isomer the variance of V(Fe,Fe) is 0.64; extrapolating to the classical limit where the square root of the variance is the standard deviation, one gets N(Fe,Fe) = 0.65 ± 0.8 (the error bar is larger than the population because the standard deviation is not a quantum mechanical observable although the variance is an observable). Moreover, the variance of the Fe core population is also very large, typically of the order of 2.75. The covariance analysis shows that the delocalization mostly involves the V(Fe,C) basins and to a lesser extent the V(Fe, Fe) and the other C(Fe) basins.

The valence basin populations of the ligands are reported in Table 3, together with the differences with respect to free CO

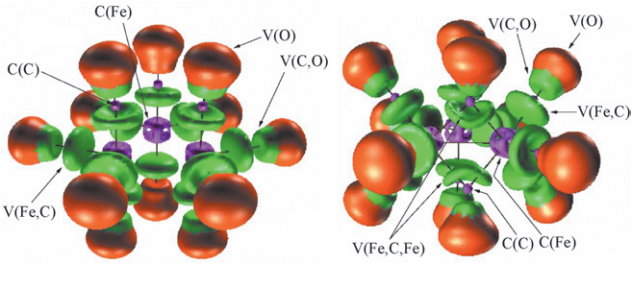

Fig. 3 Localization domains of the $Fe_3(CO)_{12}$ isomers: D_{3h} (left) and C_{2v} (right). The ELF value defining the bonding isosurface is $\eta(r)$ = 0.75. Color code: magenta = core, red = monosynaptic, green = di- and trisynaptic.

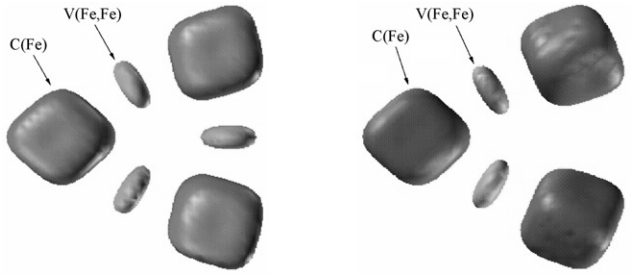

Fig. 4 Localization domains of the Fe_3 moiety of the $Fe_3(CO)_{12}$ isomers: D_{3h} (left) and C_{2v} (right). The ELF value defining the bonding isosurface is $\eta(r) = 0.30$.

and with the net electron transfer from the Fe_3 cluster. In both isomers the net electron density transfer towards CO is larger for the equatorial position than for the apical one. This is consistent with chemical intuition because the FeC distances are shorter for the equatorial position than for the apical one. In the case of the bridging position, the electron transfer is twice that in the apical position. This charge transfer corresponds to a gain of electron density in the V(Fe,C) and V(O) basins and to a loss in the V(C,O) one. This latter loss is larger in magnitude for the ligands in the apical position, which explains why the CO bond length increases more than in equatorial ligands. For bridging ligands the V(C,O) loss amounts to 0.55e, about twice the equatorial value.

It is not possible to make a direct one-to-one correspondence between the valence population analysis and the σ-donation and π-back donation provided by the Dewar–Chatt–Duncanson scheme[53,54] in the molecular orbital representation. Nonetheless, in the case of the linear MCO series (M = Sc to Cu) it has been shown that the contribution of the σ orbitals to the net transfer is very small compared to the π contribution. The analysis of the canonical orbital contribution to the valence basin is less quantitative for $Fe_3(CO)_{12}$ where the canonical orbitals are delocalized over all ligands. However, the trend observed for the MCO complexes is confirmed.[55] With respect to $Fe(CO)_5$, all population variations are enhanced in absolute value: those of the V(Fe,C) basins by about 0.1e and those of the V(C,O) and V(O) basins by about 0.02e. In the C_{2v} isomer each bridging ligand forms a three-center dative bond with the iron atoms Fe(2) and Fe(3) rather than two single bonds as there is a V(Fe,C,Fe) trisynaptic basin rather than two V(Fe,C) ones. It is worth noting that this bond is a true 4e-3c bond in the topological sense since the population of the corresponding basin is 3.43e at variance with the 4e-3c bonding scheme invoked to explain the formation of hypervalent molecules such as XeF_2.

Table 3 CO moiety basin populations N, transfers ΔN with respect to free CO, and net electron transfer δQ

	V(Fe,C)		V(C,O)		V(O)		
	N	ΔN	N	ΔN	N	ΔN	δQ
Free CO							
	2.64		3.25		4.14		
***D*$_{3h}$**							
Apical	3.04	0.40	3.02	−0.23	4.31	0.17	0.34
Equatorial	3.16	0.52	3.07	−0.18	4.35	0.21	0.55
***C*$_{2v}$**							
Fe(1) ap	2.95	0.31	3.13	−0.12	4.33	0.19	0.38
Fe(1) eq	3.16	0.52	3.12	−0.13	4.33	0.19	0.58
Fe(2) ap	3.06	0.42	3.05	−0.20	4.35	0.21	0.43
Fe(2) eq	3.12	0.48	3.13	−0.12	4.36	0.22	0.58
Fe(2) br	3.43	0.79	2.79	−0.46	4.71	0.57	0.9

The determination of the valence shell population of an atom in a molecule was recently adressed by Gillespie and Silvi on the basis of ELF topological analysis.[56] The valence population of an atom A is the sum of the populations of the monosynaptic basins V_i(A) and of the polysynaptic ones involving this center:

$$N_v(A) = \sum_i V_i(A) + \sum_{X,Y,\ldots} V(A,X,Y,\ldots)$$

However, a direct comparison between valence populations and electron counts satisfying or not the integer number of electron rules (octet, 18-electron) is not always possible because the electron counts imply that the valence electrons are arranged in one valence Lewis structure whereas the valence populations implicitly take into account the superposition of resonance structures. For example, the populations of the free carbon monoxide valence basins are explained by the superposition of 4 structures among which only one obeys the octet rule.[57] Moreover, the topological analysis assigns to Fe cores an integrated density of 23.5e instead of 18e in the standard procedure. In the D_{3h} complex, the Fe valence shell population is 13.7e (19.2e if we add the 5.5 "excess core" density) whereas in the C_{2v} structure it is 13.3e (18.8e) for Fe(1) and 16.65e (22.12e) for Fe(2/3). These results show that the 18-electron rule cannot be accounted for by our position space partition of the electron density, mostly because this rule implicitly relies on an independent particle representation in the wave function space.

4 Conclusions

The topological analysis shows that: (i) the Fe_3 cluster is not linked by 3 single bonds, but rather by a delocalized electron pair and (ii) the stabilization of the C_{2v}isomer with respect to the D_{3h} one is mostly due to the replacement of two two-center dative bonds by two three-center ones. This is accompanied by a larger charge transfer towards these bridging ligands.

References

1 C. H. Wei and L. F. Dahl, *J. Am. Chem. Soc.*, 1969, **91**, 1351.
2 F. A. Cotton and J. M. Troup, *J. Am. Chem. Soc.*, 1974, **96**, 4155.
3 D. Braga, L. Farrugia, F. Grepioni and B. F. G. Johnson, *J. Org. Chem.*, 1994, **464**, C39.
4 D. Braga, F. Grepioni, L. Farrugia and B. F. G. Johnson, *J. Chem. Soc., Dalton Trans.*, 1994, 2911.
5 T. H. Walter, L. Reven and E. Oldfield, *J. Chem. Phys*, 1989, **93**, 1320.
6 D. Braga, F. Grepioni, E. Tedesco, M. J. Calhorda and P. E. M Lopes, *J. Chem. Soc., Dalton Trans.*, 1995, 3297.
7 A. Rosa and E. J. Baerends, *New J. Chem.*, 1991, **15**, 815.
8 C. Minot and M. Criado-Sancho, *Nouv. J. Chim.*, 1984, **8**, 537.
9 J. H. Jang, J. G. Lee, H. Lee, Y. Xie and H. F. Schaefer, III, *J. Phys. Chem. A*, 1998, **102**, 5298.
10 E. Hunstock, C. Meali, M. J. Calhorda and J. Reinhold, *Inorg. Chem.*, 1999, **38**, 5053.
11 P. Hohenberg and W. Kohn, *Phys. Rev.*, 1964, **136**, B864.
12 R. G. Parr and W. Yang, *J. Am. Chem. Soc.*, 1984, **106**, 4049.
13 W. Yang and R. G. Parr, *Proc. Natl. Acad. Sci. USA*, 1985, **82**, 6723.
14 M. Berkowitz, S. K. Ghosh and R. G. Parr, *J. Am. Chem. Soc.*, 1985, **107**, 6811.
15 S. K. Ghosh and M. Berkowitz, *J. Chem. Phys.*, 1985, **83**, 2976.
16 M. Berkowitz and R. G. Parr, *J. Chem. Phys.*, 1988, **88**, 2554.
17 S. K. Ghosh, *Chem. Phys. Lett.*, 1990, **172**, 77.
18 M. K. Harbola, P. K. Chattaraj and R. G. Parr, *Isr. J. Chem.*, 1991, **31**, 395.
19 W. Langenaeker, F. De Proft and P. Geerlings, *J. Phys. Chem.*, 1995, **99**, 6424.
20 B. G. Baekelandt, A. Cedillo and R. G. Parr, *J. Chem. Phys.*, 1995, **103**, 8548.
21 F. De Proft, S. Liu and R. G. Parr, *J. Chem. Phys.*, 1997, **107**, 3000.

22 P. W. Ayers and M. Levy, *Theor. Chem. Acc.*, 2000, **103**, 353.
23 B. Silvi, *J. Phys. Chem. A*, 2003, **107**, 3081.
24 A. D. Becke and K. E. Edgecombe, *J. Chem. Phys.*, 1990, **92**, 5397.
25 D. Jayatilaka, *Phys. Rev. Lett.*, 1998, **80**, 798.
26 V. Tsirelson and A. Stash, *Chem. Phys. Lett.*, 2002, **351**, 142.
27 R. F. W. Bader, *Atoms in Molecules: A Quantum Theory*, Oxford University Press, Oxford, 1990.
28 B. Silvi and A. Savin, *Nature (London)*, 1994, **371**, 683.
29 U. Häussermann, S. Wengert and R. Nesper, *Angew. Chem., Int. Ed. Engl.*, 1994, **33**, 2073.
30 A. Savin, R. Nesper, S. Wengert and T. F. Fässler, *Angew. Chem., Int. Ed.*, 1997, **36**, 1809.
31 A. Savin, B. Silvi and F. Colonna, *Can. J. Chem.*, 1996, **74**, 1088.
32 B. Silvi, *J. Mol. Struct.*, 2002, **614**, 3.
33 R. MacWeeny, *Methods of Molecular Quantum Mechanics*, Academic Press, London, 2nd edn., 1989.
34 S. Noury, F. Colonna, A. Savin and B. Silvi, *J. Mol. Struct.*, 1998, **450**, 59.
35 X. Fradera, M. A. Austen and R. F. W. Bader, *J. Phys. Chem. A*, 1998, **103**, 304.
36 J. Cioslowski and S. T. Mixon, *J. Am. Chem. Soc.*, 1991, **113**, 4142.
37 J. G. Ángyán, M. Loos and I. Mayer, *J. Phys. Chem.*, 1994, **98**, 5244.
38 A. D. Becke, *J. Chem. Phys.*, 1993, **98**, 5648.
39 A. D. Becke, *Phys. Rev .A*, 1988, **38**, 3098.
40 C. Lee, Y. Yang and R. G. Parr, *Phys. Rev. B*, 1988, **37**, 785.
41 B. Miechlich, A. Savin, H. Stoll and H. Preuss, *Chem. Phys. Lett.*, 1989, **157**, 200.
42 M. J. Frisch, G. W. Trucks, H. B. Schlegel, G. E. Scuseria, M. A. Robb, J. R. Cheeseman, V. G. Zakrzewski, J. A. Montgomery, Jr., R. E. Stratmann, J. C. Burant, S. Dapprich, J. M. Millam, A. D. Daniels, K. N. Kudin, M. C. Strain, O. Farkas, J. Tomasi, V. Barone, M. Cossi, R. Cammi, B. Mennucci, C. Pomelli, C. Adamo, S. Clifford, J. Ochterski, G. A. Petersson, P. Y. Ayala, Q. Cui, K. Morokuma, D. K. Malick, A. D. Rabuck, K. Raghavachari, J. B. Foresman, J. Cioslowski, J. V. Ortiz, A. G. Baboul, B. B. Stefanov, G. Liu, A. Liashenko, P. Piskorz, I. Komaromi, R. Gomperts, R. L. Martin, D. J. Fox, T. Keith, M. A. Al-Laham, C. Y. Peng, A. Nanayakkara, M. Challacombe, P. M. W. Gill, B. Johnson, W. Chen, M. W. Wong, J. L. Andres, C. Gonzalez, M. Head-Gordon, E. S. Replogle and J. A. Pople, *Gaussian 98, Revision A.9*, Gaussian Inc., Pittsburgh, PA, 1998.
43 T. Clark, J. Chandrasekhar, G. W. Spitznagel and P. von Ragué Schleyer, *J. Comput. Chem.*, 1983, **4**, 294.
44 M. J. Frisch, J. A. Pople and J. S. Binkley, *J. Chem. Phys.*, 1984, **80**, 3265.
45 A. D. MacLean and G. S. Chandler, *J. Chem. Phys.*, 1980, **72**, 5639.
46 R. Krishnan, J. S. Binkley, R. Seeger and J. A. Pople, *J. Chem. Phys.*, 1980, **72**, 650.
47 S. Noury, X. Krokidis, F. Fuster and B. Silvi, ToPMoD Package, Laboratoire de Chimie Théorique de l'Université Pierre et Marie Curie, Paris, France, 1997.
48 S. Noury, X. Krokidis, F. Fuster and B. Silvi, *Comput. Chem.*, 1999, **23**, 597.
49 E. Pepke, J. Murray, J. Lyons and T.-Z. Hwu, SciAn software, Supercomputer Computations Research Institute, Florida State University, Tallahassee, FL, 1993.
50 D. Braga, F. Grepioni and A. G. Orpen, *Organometallics*, 1993, **12**, 1481.
51 L. H. Jones, R. S. McDowell, M. Goldblatt and B. I. Swanson, *J. Chem. Phys.*, 1972, **57**, 2050.
52 R. Bianchi, G. Gervasio and D. Marabello, *Inorg. Chem.*, 2000, **39**, 2360.
53 M. J. S. Dewar, *Bull. Soc. Chim.*, 1951, **18**, c79.
54 J. Chatt and L. A. Duncanson, *J. Chem. Soc.*, 1953, 2939.
55 J. Pilme, I. Alikhani and B. Silvi, *J. Phys. Chem. A*, 2003, **107**, 4500.
56 R. J. Gillespie and B. Silvi, *Coord. Chem. Rev.*, 2002, **233–234**, 53.
57 C. Lepetit, B. Silvi and R. Chauvin, *J. Phys. Chem. A*, 2003, **107**, 464.